scientific reports



OPEN

Stability and repeatability of diffusion-weighted imaging (DWI) of normal pancreas on 5.0 Tesla magnetic resonance imaging (MRI)

Zhiyong Jiang^{1,4}, Wenbo Sun^{1,4}, Dan Xu¹, Hao Yu¹, Hao Mei¹, Xiaopeng Song^{2,3}& Haibo Xu¹

To explore the stability and repeatability of diffusion-weighted imaging (DWI) of normal pancreas with different field of views (FOV) on 5.0 T magnetic resonance imaging (MRI) system. Twenty healthy subjects underwent two sessions of large FOV (IFOV) and reduced FOV (rFOV) DWI sequence scanning. Two radiologists measured the apparent diffusion coefficient (ADC) values and the signal-to-noise ratio (SNR) of the pancreatic head, body, and tail on DWI images, simultaneously, using a 5-point scale, evaluate the artifacts and image quality. One radiologist re-measured the ADC on DWI images again after a 4-week interval. The test-retest repeatability of two scan sessions were also evaluated. Intra-observer and inter-observer at IFOV and rFOV, the ADC values were not significantly different (P>0.05), intraclass correlation coefficients (ICCs) and coefficient of variations were excellence (ICCs 0.85–0.99, CVs < 8.0%). The ADC values were lower with rFOV than IFOV DWI for the head, body, tail, and overall pancreas. The consistency of the two scan sessions were high. The high stability and repeatability of pancreas DWI has been confirmed at 5.0 T. Scan durations are reduced while resolution and image quality are improved with rFOV DWI, which is more preferable than IFOV for routine pancreas imaging.

Abbreviations

DWI Diffusion-weighted image ADC Apparent diffusion coefficient

IFOV Large field of view rFOV Reduced field of view

MRI Magnetic resonance imaging

SNR Signal-to-noise ratio

Magnetic resonance imaging (MRI) is an essential tool for diagnosing pancreatic pathologies, including pancreatitis and pancreatic cancer^{1,2} However, imaging the pancreas by MRI is challenging due to its small size, respiratory motion and gas in the surrounding stomach and bowel³. This location of pancreas creates an uneven distribution of the B0 and B1+ fields, resulting in significant signal loss that makes improving the resolution and robustness of quantitative imaging in the pancreas a difficult task⁴.

Diffusion-weighted imaging (DWI) is a functional MRI sequence that can provide information on the diffusion of water molecules within biological tissues^{5,6}. Apparent diffusion coefficient (ADC) is a quantitative measure derived from DWI, and has been increasingly used to evaluate and diagnose pancreatic pathologies⁷. In pancreatic imaging, ADC values have been found to be useful in differentiating between benign and malignant pancreatic lesions, as well as monitoring treatment response in pancreatic cancer patients^{8–10}. One of the

¹Department of Radiology, Zhongnan Hospital of Wuhan University, 169 Donghu Rd, Wuchang District, Wuhan, Hubei, China. ²United Imaging Healthcare, Shanghai, China. ³Wuhan Zhongke Industrial Research Institute of Medical Science, Wuhan, Hubei, China. ⁴These authors contributed equally: Zhiyong Jiang and Wenbo Sun [™]email: xiaopenq.song@wh-iri.orq.cn; xuhaibo@whu.edu.cn

advantages of ADC value is its stability, as it is generally not affected by equipments or sequence parameters¹¹. This stability is due to the fact that ADC value is a basic property of the tissue being imaged. However, ADC values may also be subject to variations due to biological factors, technical factors and measurement errors. For instance, increasing spatial resolution can lead to a rapid decrease in the signal-to-noise ratio (SNR) of DWI, which may result in a noise floor bias in ADC measures. Therefore, the spatial resolution of DWI is poor, which limited its application in pancreatic imaging.

Magnetic resonance reduced field of view (rFOV) imaging is a technique that overcomes resolution challenges and improves visualization of the pancreas¹². The rFOV technique reduces the field of view in MRI imaging, resulting in higher spatial resolution and better imaging quality 13-16. By reducing the field of view, rFOV-DWI imaging improves visualization of small structures, and minimizes signal loss caused by the inhomogeneous B1 + field distribution in the pancreas region¹⁷. Moreover, rFOV-DWI imaging targets specific regions of interest in the pancreas, improving detection and characterization of pancreatic pathologies 18. In addition, high-field MRI at 3.0 Tesla (3.0 T) has become increasingly popular in clinical practice to improve the resolution of pancreatic MRI. Compared to traditional 1.5 Tesla (1.5 T) MRI, 3.0 T MRI offers several advantages in pancreatic imaging. One of the main advantages of 3.0 T MRI is its ability to provide better tissue contrast, which is particularly important in pancreatic imaging where it can be challenging to differentiate between pancreatic lesions and surrounding normal tissues. Another advantage of 3.0 T MRI is its higher SNR, which allows for better spatial resolution, improving detection and characterization of small pancreatic lesions and diagnostic accuracy. Combining high-field MRI with rFOV-DWI is an important diagnostic direction for the pancreas. Studies by Ma et al. and Kim et al. have shown that 3.0 T rFOV-DWI improves resolution by a factor of 2 compared to large-FOV (IFOV) DWI^{12,19}. Donati et al. also reported higher image quality, anatomic detail, and lesion detection using rFOV-DWI versus lFOV-DWI of the pancreas on 3.0 T MRI²⁰.

The clinical application of a newly developed 5.0 T magnetic resonance imaging (MRI) system in pancreas diagnostics has yet to be fully evaluated. Specifically, there is a lack of research on the quality, stability, and repeatability of IFOV and rFOV DWI on a 5.0 T MRI. Given that higher magnetic field strengths can lead to increased artifacts, particularly in the abdomen where the radiofrequency (RF) wavelength is shorter, it is crucial to investigate the repeatability of IFOV and rFOV DWI of pancreas at 5.0 T. Additionally, a comparison of the quality and consistency between IFOV and rFOV ADC is warranted. Our study aimed to assess the clinical utility of 5.0 T MRI for pancreas imaging and to explore the feasibility of using rFOV to enhance ADC image quality.

Materials and method

Subjects. Twenty healthy subjects participated in the prospective investigation and underwent MRI scanning of the pancreas between February 2022 and May 2022. This study was approved by the local Ethics Committee. All volunteers signed the informed consent form. Included if: (1) individuals aged 18–65; (2) no history of drug abuse, drug use one week before the exam, pancreatitis, diabetes, alcohol abuse, chronic liver diseases, hepatic steatosis, or abdominal surgery; (3) no contraindications for MRI (such as implanted pacemaker, metallic implant, and claustrophobia). Exclusion criteria: (1) incomplete DWI procedure due to any reasons, (2) poor image quality (with high motion artifacts) unsuitable for further imaging analysis.

MRI scanning. The 5.0 T whole-body magnetic resonance scanning system (uMR Jupiter, United-Imaging Healthcare, Shanghai, China) was used for all MRI examinations in this study, using a flexible 24-channel body coil and the built-in 24-channel spine coil. Table 1 showed the scanning parameters.

For regular IFOV DWI scanning, the parameters were field of view (FOV): 300×380 mm²; voxel: $2.38 \times 2.38 \times 4$ mm³; repetition time (TR): ~ 3833 ms; echo time (TE): 49.7 ms; bandwidth (BW): 2300 kHz; slice thickness: 4 mm; number of slices: 16; b values: 0 s/mm^2 (average time = 1), and 800 s/mm^2 (average time = 5); parallel imaging acceleration factor: 3; and scanning time: $\sim 200 \text{ s}$.

	lFOV_T2	lFOV_DWI	rFOV_DWI
TR (ms)	~ 6537	~ 3833	~ 3555
TE (ms)	74.88	49.7	49.7
Flip angle	90°	90°	90°
Field of view (FOV)	300×380	300×380	120×240
In-plane resolution (mm ²⁾	1.47×1.25	2.38×2.38	1.5×1.5
Matrix	204×304	126×160	80×160
Receiver bandwidth (kHz)	260	2300	2300
Slice thickness (mm)	6	4	4
No. of slices	24	16	16
Acceleration factor	2	2	2
Echo train length	13	51	48
B-values		0, 800	0, 800
Average times	1	1, 5	1,5
Total acquisition duration (s)	~252	~200	~125

Table 1. MR imaging sequence parameters.

For rFOV DWI scanning, the parameters were FOV: $120 \times 240 \text{ mm}^2$; voxel: $1.50 \times 1.50 \times 4 \text{ mm}^3$; TR: 3555 ms; TE: 49.7 ms; BW; 2300 kHz; slice thickness: 4 mm; number of slices: 16; b values: 0 s/mm^2 (average time = 1), and 800 s/mm^2 (average time = 5); parallel imaging acceleration factor: 3; and scanning time: 125 s.

All subjects were fasted for at least 6 hours before the MRI examination. Each subject underwent two sessions of MRI scanning, after the first scanning session was completed, the second scanning session was performed after an interval of about 48 hours, and the sequence parameters and positioning for scanning were the same as the first session. For each scanning session, after shimming, each subject first underwent IFOV T2 scanning, and then IFOV DWI scanning, afterward, rFOV DWI scanning was performed and got the images (Fig. 1). The respiration-triggered scanning method (end-expiration triggering) was used.

Data analysis. The MRI images of all participants were analyzed by the same two radiologists with 12 and 15 years of experience, respectively. The distribution of SNR and ADC values of manually selected regions of interest (ROIs) were examined. ROIs were selected from pancreatic head (from the margin of the right to the left superior mesenteric vein), pancreatic body (pancreas region from the left margin of the superior mesenteric vein to the left aorta), and tail (pancreas region from the left margin of the aorta to the hilus lienis). The pancreatic ducts, cystic lesions, or artifacts were avoided when choosing the ROIs. ROI was placed at least 6 mm from the pancreas margin to avoid the average volume effect.

For objectively assessing the signal-to-noise ratio (SNR) and ADC variability, the two radiologists delineated the ROIs of the pancreatic head, body, and tail on DWI images independently. One radiologist (observer 1) delineated the ROIs and re-measured the SNR and ADC on DWI images again after a 4-week interval. rFOV images do not include any areas outside of the body; therefore, air cannot be utilized in the calculation of SNR. SNR was calculated as the ratio between the average signal intensity and the standard deviation of the signal intensity manually placed circular ROIs. The average ADC value was acquired from the oval/round ROI on ADC images. The areas of ROI ranged from 50 to 100 mm². The average ADC values of the pancreatic head, body, and tail were calculated as the overall ADC value of the pancreas.

The semi-quantitative grading system was used to evaluate image quality and artifact grade. The presence of artifacts was first assessed, and then two radiologists independently assessed the IFOV and rFOV DWI images using the 5-level criteria (5, no artifacts; 4, low amounts of artifacts not influencing the quality of diagnosis; 3, with artifacts that could reduce the quality of diagnosis; 2, with artifacts leading to the minimal information of diagnosis; and 1, could not be used for diagnosis). A subjective assessment of overall image quality was also performed (5, the best image quality; 4, high image quality for diagnosis; 3, images with limited diagnostic value/quality; 2, images provide only very limited information for diagnosis; and 1, could not be used for diagnosis).

Statistical analysis. SPSS 26.0 was used for statistical analysis. The Shapiro–Wilk test was performed for the normality test. Continuous data with a normal distribution were described as means \pm standard deviations and analyzed using the independent sample t-test. The paired t-test was used for the comparisons between the two measurements of ADC and SNR from the same investigator. Normality and Lognormality Tests are used to analyze the ADC value between rFOV and lFOV. Intra- and inter-observer variability and test–retest repeatability (the reprocucibility of two scanning sessions) of ADC measurements for each anatomical region of the pancreas and whole pancreas were analyzed by the Bland–Altman analysis, coefficient of variation (CV), and intra-class correlation coefficient (ICC). The Bland–Altman test and weighted κ coefficient was used to analyze the consistency of ADC between lFOV and rFOV. P < 0.05 was considered statistically significant.

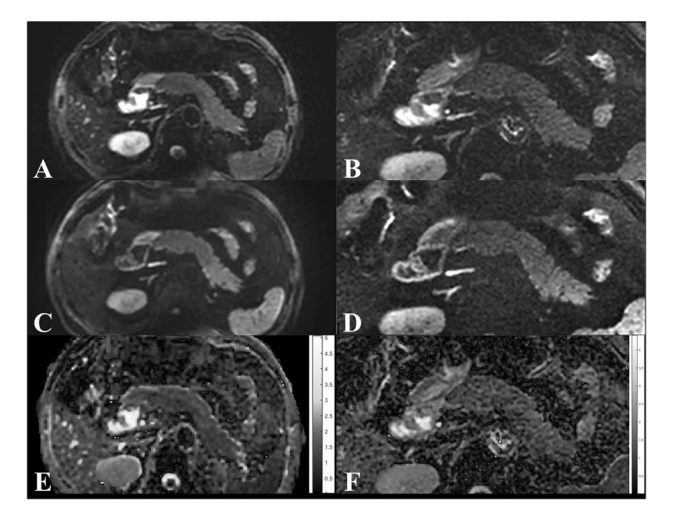


Figure 1. Male, 57 years old. IFOV: b0 (A), b800 (C), ADC map (E). rFOV: b0 (B), b800 (D), ADC map (F).

Ethics approval. The study was conducted in accordance with the Declaration of Helsinki, and approved by the institutional review board of Zhongnan Hospital, Wuhan University (No.2021095, December 2021). The subjects in the study provided written informed consent.

Results

Subject information. Twenty-two individuals underwent MRI scanning in this study. One was excluded due to severe artifacts, and another was excluded for not acquiring data in the scanning process. Finally, 20 volunteers were included in the analysis, of which 13 were males and 7 were females. The ages of the males and females were 48.9 ± 14.0 and 45.9 ± 15.5 years old, respectively.

ADC pancreatic evaluation (head, body, tail). The ADC values of the pancreas, measured by two observers on a total of twenty subjects. Table 2 reported the mean and standard deviation for the head, body, and tail segments of the test and retest data. Tables 3 and 4 reported that of the intra-observer and inter-observer data There was no significant difference between the two ADC measurements made by the same observer for the whole or parts of the pancreas (P > 0.05), when comparing two different observers, significant differences in ADCs were observed for the tail in IFOV (P = 0.014), the body in rFOV (P = 0.042). The normal distribution of ADCs for fFOV and rFOV is demonstrated in Fig. 2.

Test–retest repeatability. Test–retest/Scan-rescan repeatability ADC in the head, body, and tail segments were been given by Table 2. ADC repeatability showed excellent in IFOV (ICC 0.884–0.995, CV 2.9–5.1%), ADC repeatability showed good in rFOV (ICC 0.789–0.839, CV 9.5–12.4%). Corresponding Bland–Altman plots are shown in Fig. 3.

Intraobserver and interobserver repeatability. The ADCs in IFOV and rFOV showed excellent intra-observer reproducibility and inter-observer agreement (with ICCs 0.846–0.992 and CVs 2.3–8.0% inter-observer, with ICCs 0.902–0.992 and CVs 1.9–6.5% intra-observer) for the head, body, tail, and whole pancreas in IFOV and rFOV, respectively (Tables 3, 4 and Fig. 4).

SNR and subjective evaluation. SNR values were around 1.13-1.17 times higher with IFOV than rFOV for the head $(20.286 \pm 3.907 \text{ vs. } 17.924 \pm 4.485 \text{ dB})$, the body $(20.157 \pm 5.710 \text{ vs. } 17.842 \pm 4.908 \text{ dB})$, and the tail

	Test	Retest	P	ICC	CV
IFOV					
Head	1.374±0.195	1.381 ± 0.199	0.553	0.959	4.0%
Body	1.352 ± 0.151	1.372 ± 0.157	0.268	0.879	5.1%
Tail	1.289 ± 0.149	1.282 ± 0.162	0.337	0.884	2.9%
Whole pancreas	1.338 ± 0.145	1.345 ± 0.151	0.497	0.898	3.2%
rFOV					
Head	1.132 ± 0.222	1.186±0.231	0.109	0.799	12.4%
Body	1.173 ± 0.222	1.179±0.194	0.851	0.839	11.8%
Tail	1.124±0.175	1.154±0.188	0.314	0.789	11.2%
Whole pancreas	1.143 ± 0.179	1.173 ± 0.189	0.267	0.817	9.5%

Table 2. Comparing the pancreatic ADC values ($\times 10^{-3}$ mm²/s) of lFOV and rFOV various anatomic locations for Test-Retest of two scan swssions.

	1st	2nd	P value	ICC	CV	
IFOV						
Head	1.371 ± 0.191	1.381 ± 0.175	0.302	0.971	3.0%	
Body	1.354±0.184	1.345 ± 0.163	0.299	0.954	2.8%	
Tail	1.262 ± 0.154	1.298 ± 0.149	0.662	0.981	2.3%	
Whole pancreas	1.329 ± 0.147	1.350 ± 0.138	0.207	0.976	2.1%	
rFOV						
Head	1.164±0.186	1.176±0.146	0.883	0.987	1.9%	
Body	1.142 ± 0.222	1.154 ± 0.212	0.179	0.992	2.4%	
Tail	1.116±0.176	1.138 ± 0.169	0.867	0.908	6.5%	
Whole pancreas	1.141 ± 0.180	1.136±0.169	0.604	0.902	6.4%	

Table 3. Comparing the pancreatic ADC values $(\times 10^{-3} \text{ mm}^2/\text{s})$ of lFOV and rFOV at various anatomic locations for intra-observer concordance in Observer 1.

	Observer1	Observer2	P value	ICC	CV	
lFOV	lFOV					
Head	1.371 ± 0.167	1.381 ± 0.174	0.284	0.968	3.2%	
Body	1.359±0.135	1.373 ± 0.142	0.172	0.946	4.2%	
Tail	1.295 ± 0.459	1.278 ± 0.148	0.014	0.981	2.5%	
Whole pancreas	1.342 ± 0.132	1.335 ± 0.137	0.351	0.974	2.3%	
rFOV						
Head	1.175 ± 0.172	1.166 ± 0.167	0.099	0.991	2.5%	
Body	1.146 ± 0.208	1.159 ± 0.215	0.042	0.992	2.5%	
Tail	1.142 ± 0.159	1.120 ± 0.171	0.216	0.899	6.8%	
Whole pancreas	1.145 ± 0.160	1.158 ± 0.174	0.538	0.846	8.0%	

Table 4. Comparing the pancreatic ADC values ($\times 10^{-3}$ mm²/s) of lFOV and rFOV at various anatomic locations for inter-observer concordance.

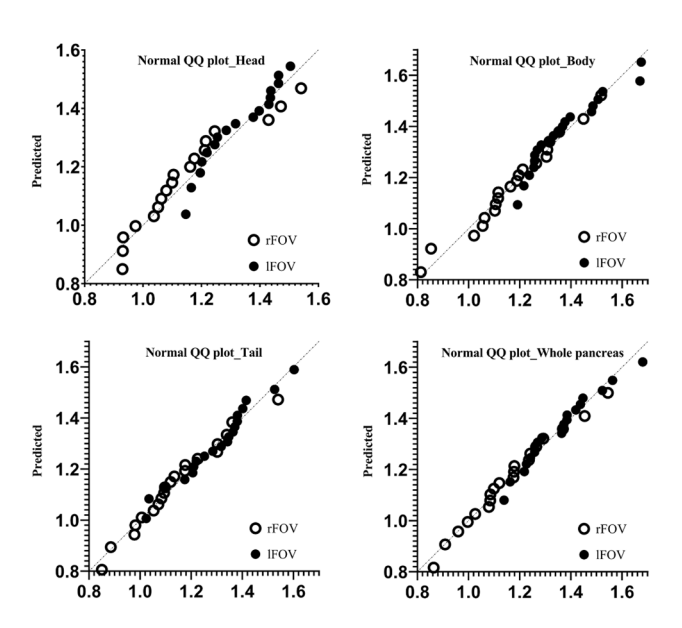


Figure 2. Normality and Lognormality Tests of QQ graph between IFOV and rFOV. In comparison to the body, the tail, and the whole pancreas, the normal distribution of ADC values in the head's rFOV and IFOV is somewhat inferior.

 $(19.418 \pm 5.057 \text{ vs. } 16.626 \pm 3.903 \text{ dB})$ in Table 5. Two observers' subjective evaluations indicate that rFOV is considerably superior to lFOV in terms of artifact evaluation and image quality evaluation (Table 6 and Fig. 5).

Discussion

The aim of this study was to assess the stability and repeatability of IFOV and rFOV DWI of pancreas at $5.0~\mathrm{T}$ by examining and comparing ADC values. In test-retest experiments, ADC repeatability showed good to excellent (ICC 0.789-0.995, CV 2.9%-12.4%). Intra-observer ADC consistency was excellent (ICC 0.902-0.992, CV 1.9-6.5%), while inter-observer ADC consistency was also excellent (ICC 0.846-0.992, CV 2.3-8.0%). Additionally, we found that the SNR of the rFOV was comparable to that of the IFOV, but the rFOV was superior to the IFOV in terms of subjective evaluation and had a shorter scanning time. These findings suggest that rFOV is more favorable for routine pancreas diagnostic imaging on a $5.0~\mathrm{T}$ MRI.

The apparent diffusion coefficient (ADC) is a crucial parameter for evaluating microstructural changes in tissues, organs, and lesions^{21,22}. Evaluating the repeatability of ADC values in diffusion-weighted imaging (DWI) is clinically important, as patients may undergo multiple DWI examinations to monitor a treatment effect or follow up on a lesion²³. Ensuring low intra- and inter-observer ADC CV is a desirable goal. Although ADC repeatability has been examined for various organs, including the breast, lung, and liver, data are limited for the pancreas^{24–27}. Our study found that the intra- and inter-observer ADC CVs were comparable to a previous study that reported mean ADC CVs of 10.6% for the whole pancreas in 3.0 T DWI examinations²⁸. Another study reported CVs of 9%, 8%, and 8% for the head, body, and tail of the pancreas²⁹. Additionally, two studies reported good ADC reproducibility of the pancreas at 1.5 and 3.0 T^{30,31}. However, discrepancies between studies may be due to differences in DWI sequence parameters, including the selection of b-values³², as well as respiration compensation acquisition and post-processing methods, which can affect ADC values³³.

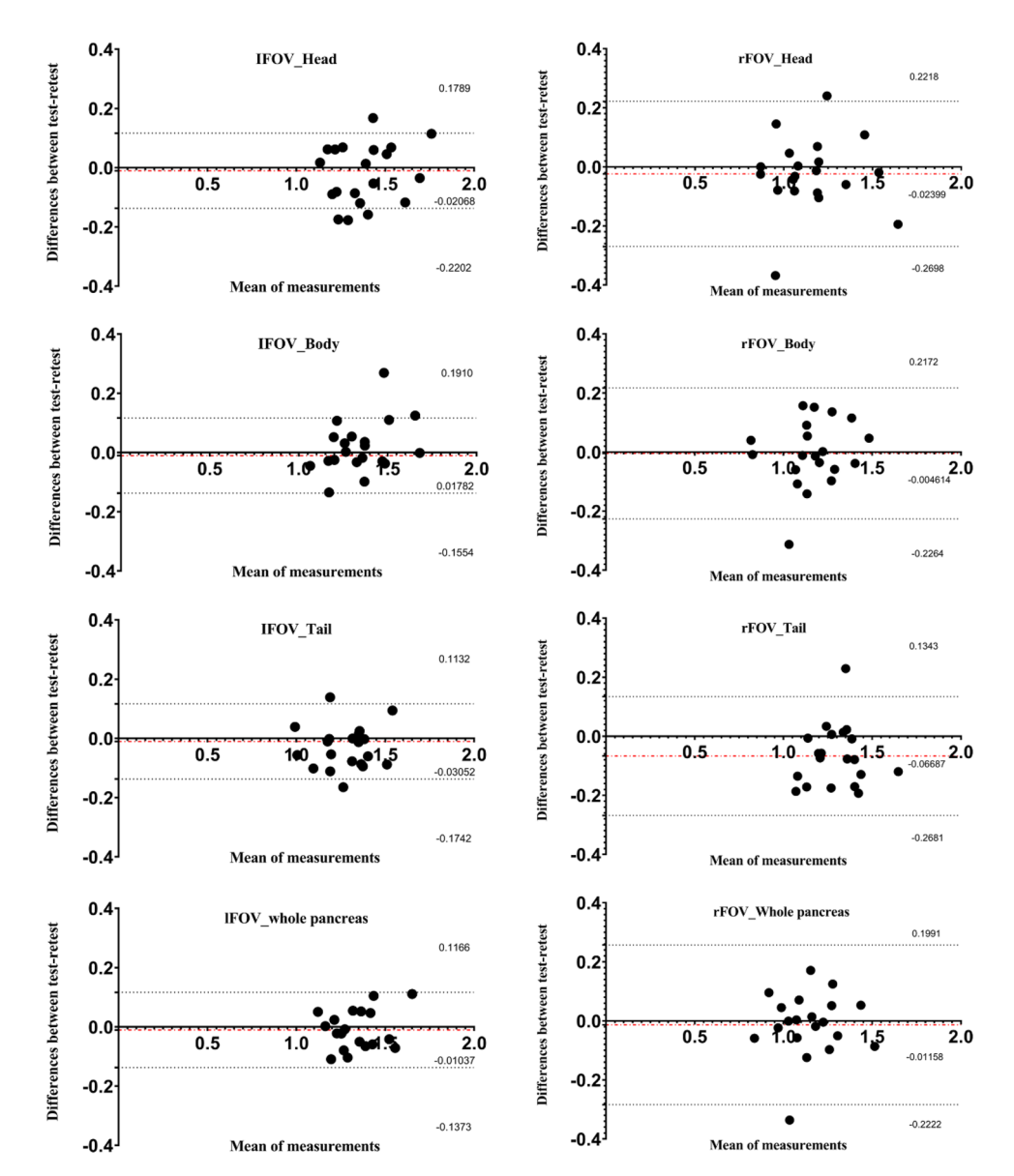


Figure 3. Test–retest reproducibility of ADC values for the 3 pancreatic segments and the whole pancreas. Bland–Altman plots of differences in test-ADC measurements (y-axis) against the retest-ADC measurement (x-axis), with a mean absolute difference (bias) (red dashed lines) and 95% confidence intervals of the mean difference (limits of agreement, LOA) (black dashed lines).

The 5.0 T MRI is a novel system that has recently become available for clinical diagnosis. However, there are few studies that have investigated 5.0 T rFOV-DWI. Zhang et al. has shown no significant differences in IFOV-DWI ADC values between 3.0 T and 5.0 T magnets in nine volunteers³4. The MRI protocol in Zhang et al. was similar to that used in our study, and their whole-pancreas ADC values $(1.394\pm0.130\times10^{-3}~\text{s/mm}^2)$ were comparable to those in our study $(1.342\pm0.132\times10^{-3}~\text{mm}^2/\text{s})$, and in previous 3.0 T studies $(1.416\pm0.175\times10^{-3}~\text{mm}^2/\text{s})$, while another study by Zheng et al. showed significant higher ADC values $(1.671\pm0.226\times10^{-3}~\text{s/mm}^2)$ in pancreas than our findings³5. This could be due to a different choice of spatial resolution in sequence parameters and a partial volume effect.

In our study, the ADC values of the pancreatic tail were found to be the lowest, which is consistent with previous reports^{29,36}. Due to the lower ADC values, even small variations can lead to higher CV compared to higher ADC values. The pancreas is approximately 15 cm long and located behind the stomach, which may lead to gradient nonlinearity and affect ADC values^{37,38}. Additionally, previous quality control studies have reported significant ADC errors for scanning areas away from the magnet isocenter³⁹. Anatomical investigations have revealed that the head, body, and tail of the pancreas have distinct cellular compositions⁴⁰. These factors may all contribute to higher CVs of the pancreatic tail.

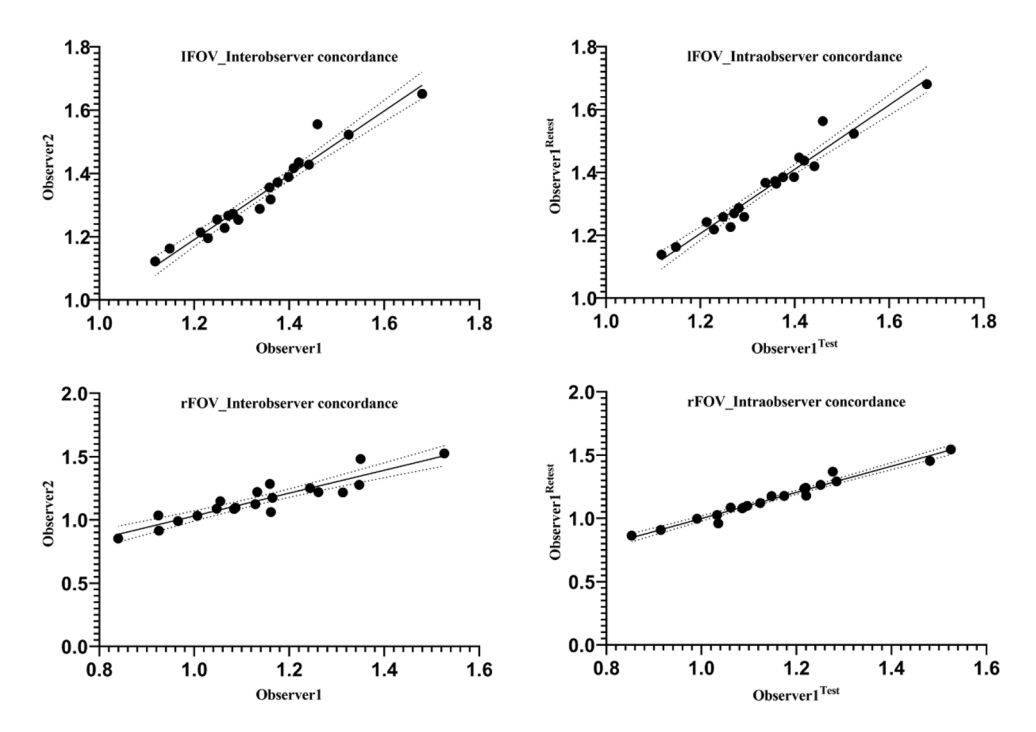


Figure 4. Scatter plot of intra-observer and inter-observer correlations. Results show excellent inter-observer and intra-observer agreement both in IFOV and rFOV.

	lFOV	rFOV	P value
SNR head	20.286 ± 3.907	17.924 ± 4.485	0.005
SNR body	20.157 ± 5.710	17.842 ± 4.908	0.057
SNR tail	19.418 ± 5.057	16.626 ± 3.903	0.019

Table 5. SNR comparisons of IFOV and rFOV.

In addition, our study found that the ADC values measured with rFOV were lower than those with IFOV, which is in line with several earlier studies^{15,17}. This phenomenon may be attributable to various factors. Firstly, the resolution of the rFOV DWI series is substantially higher than that of the IFOV sequence, which reduces the number of hydrogen spins contained in a single voxel, resulting in lower transverse magnetization and less information being gathered⁴¹. Secondly, due to the smaller FOV, certain external and adjacent tissue and organ signals outside of the FOV are filtered out, whereas these signals may contribute to higher ADC values in a large FOV DWI. Lastly, the modalities of RF excitation for rFOV and IFOV DWI sequences are different, and rFOV DWI may be more sensitive to abdominal movement and other physiological noise.

Limitations. There are several limitations to the current study. Firstly, the sample size was small, and all participants were healthy. Thus, it is unclear whether the results can be generalized to pancreas lesions. Secondly, it would have been preferable to include several repeated assessments instead of just two repeated examinations to accurately assess the repeatability of the measurements. Thirdly, the study only demonstrated short-term reproducibility of DWI on ultra-high field MRI, which limits the ability to evaluate all potential factors of long-term variability.

Conclusions

Our study demonstrated high stability, repeatability, and consistency of ADC values for the pancreas in both IFOV and rFOV at 5.0 T DWI sequences. Moreover, rFOV DWI showed improved resolution and image quality while reducing scan duration. Therefore, 5.0 T DWI may serve as a reliable tool for clinical diagnosis of pancreas diseases, and rFOV DWI is a feasible quantitative imaging tool for investigating lesions and changes of the pancreas in clinical settings.

Parameter	IFOV	rFOV	P value			
1 urumeter	пот	1101	1 varue			
Image artifacts						
Observer 1	3.450 ± 0.510	4.100 ± 0.447	0.031			
Observer 2	3.850 ± 0.587	4.600 ± 0.503	0.001			
ICC	0.588	0.421	N/A			
Overall image quality						
Observer 1	3.500 ± 0.607	4.250 ± 0.550	0.000			
Observer 2	3.750 ± 0.444	4.550 ± 0.510	0.002			
ICC	0.488	0.422	N/A			

Table 6. Image artifacts and overall image quality scores.

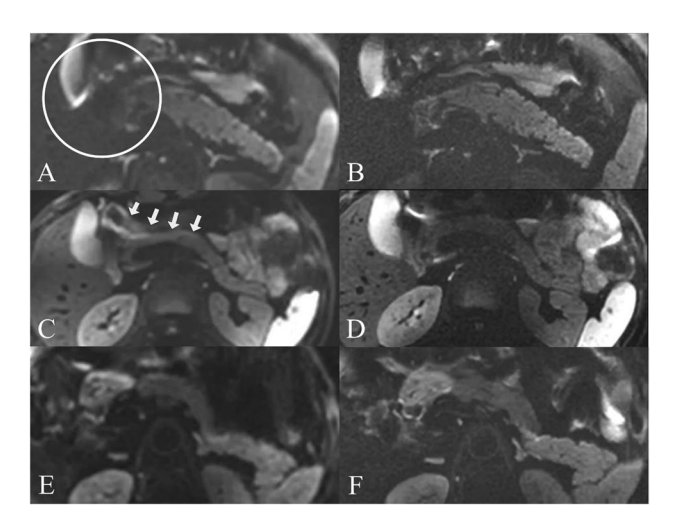


Figure 5. b800 of IFOV (**A**, **C**, **E**), b800 of rFOV (**B**, **D**, **F**). According to the image, rFOV images have a greater resolution and more clear contours than IFOV images. In **A**, **B**, on the b800 DWI image of IFOV, as depicted by the white solid circle, the head of the pancreas is obscured by the adjacent gallbladder and surrounding intestines, and the partial display is not clear. In **C**, **D**, the position shown by the white pointed head, the pancreas appears pseudo-diffusion-restricted in IFOV due to the convolution effect of the surrounding intestine, this effect disappears in rFOV DWI. In **E**, **F**, demonstrate that the diffuse look of the body and tail of the pancreas on DWI images is distinct, because of that the head, body, and tail of the pancreas have distinct cellular compositions.

Data availability

The datasets used and/or analysed during the current study available from the corresponding author on reasonable request.

Received: 12 January 2023; Accepted: 6 July 2023 Published online: 24 July 2023

References

- 1. Best, L. M., Rawji, V., Pereira, S. P., Davidson, B. R. & Gurusamy, K. S. Imaging modalities for characterising focal pancreatic lesions. *Cochrane Database Syst. Rev.* 4(4), CD010213 (2017).
- 2. Lee, E. S. & Lee, J. M. Imaging diagnosis of pancreatic cancer: A state-of-the-art review. World J. Gastroenterol. 20(24), 7864–7877 (2014).
- 3. Harrington, K. A., Shukla-Dave, A., Paudyal, R. & Do, R. K. G. MRI of the pancreas. J. Magn. Reson. Imaging 53(2), 347-359 (2021).
- 4. Hill, D. V. & Tirkes, T. Advanced MR Imaging of the pancreas. Magn. Reson. Imaging Clin. N. Am. 28(3), 353–367 (2020).
- 5. Le Bihan, D. *et al.* MR imaging of intravoxel incoherent motions: application to diffusion and perfusion in neurologic disorders. *Radiology* **161**(2), 401–407 (1986).
- 6. Higaki, T. *et al.* Introduction to the technical aspects of computed diffusion-weighted imaging for radiologists. *Radiographics* **38**(4), 1131–1144 (2018).
- 7. Ma, W. et al. Apparent diffusion coefficient and dynamic contrast-enhanced magnetic resonance imaging in pancreatic cancer: Characteristics and correlation with histopathologic parameters. J. Comput. Assist. Tomogr. 40(5), 709–716 (2016).
- 8. Lotfalizadeh, E. et al. Prediction of pancreatic neuroendocrine tumour grade with MR imaging features: added value of diffusion-weighted imaging. Eur Radiol. 27(4), 1748–1759 (2017).
- 9. Hong, B. Z., Li, X. F. & Lin, J. Q. Differential diagnosis of pancreatic cancer by single-shot echo-planar imaging diffusion-weighted imaging. World J. Gastroenterol. 21(20), 6374–6380 (2015).

- 10. Niu, X. et al. Value of diffusion-weighted imaging in distinguishing pancreatic carcinoma from mass-forming chronic pancreatitis: A meta-analysis. Chin. Med. J. (Engl). 127(19), 3477–3482 (2014).
- Fedeli, L. et al. Italian association of physics in medicine (AIFM) working group on MR Intercomparison. Dependence of apparent diffusion coefficient measurement on diffusion gradient direction and spatial position—a quality assurance intercomparison study of forty-four scanners for quantitative diffusion—weighted imaging. Phys. Med. 55, 135–141 (2018).
- 12. Ma, C. et al. High resolution diffusion weighted magnetic resonance imaging of the pancreas using reduced field of view single-shot echo-planar imaging at 3 T. Magn. Reson. Imaging 32(2), 125–131 (2014).
- 13. Thierfelder, K. M. *et al.* Diffusion-weighted MRI of the prostate: Advantages of Zoomed EPI with parallel-transmit-accelerated 2D-selective excitation imaging. *Eur. Radiol.* **24**(12), 3233–3241 (2014).
- 14. Brendle, C. et al. Diffusion-weighted imaging in the assessment of prostate cancer: Comparison of zoomed imaging and conventional technique. Eur. J. Radiol. 85(5), 893–900 (2016).
- Cai, J. S. et al. Reduced field-of-view diffusion-weighted imaging (DWI) in patients with gastric cancer: Comparison with conventional DWI techniques at 3.0T: A preliminary study. Medicine 99(1), e18616 (2020).
- Chen, M. et al. Comparison of reduced field-of-view diffusion-weighted imaging (DWI) and conventional DWI techniques in the assessment of Cervical carcinoma at 3.0T: Image quality and FIGO staging. Eur. J. Radiol. 137, 109557 (2021).
- 17. Mannelli, L. et al. Comparison of navigator triggering reduced field of view and large field of view diffusion-weighted imaging of the pancreas. J. Comput. Assist. Tomogr. 43(1), 143–148 (2019).
- 18. He, M. et al. Prospective comparison of reduced field-of-view (rFOV) and full FOV (fFOV) diffusion-weighted imaging (DWI) in the assessment of insulinoma: Image quality and lesion detection. Acad Radiol. 27(11), 1572–1579 (2020).
- 19. Kim, H. et al. Reduced field-of-view diffusion-weighted magnetic resonance imaging of the pancreas: Comparison with conventional single-shot echo-planar imaging. Korean J. Radiol. 16(6), 1216–1225 (2015).
- 20. Donati, F., Casini, C., Cervelli, R., Morganti, R. & Boraschi, P. Diffusion-weighted MRI of solid pancreatic lesions: Comparison between reduced field-of-view and large field-of-view sequences. *Eur. J. Radiol.* 143, 109936 (2021).
- Zhu, M. et al. Accuracy of quantitative diffusion-weighted imaging for differentiating benign and malignant pancreatic lesions: A systematic review and meta-analysis. Eur. Radiol. 31(10), 7746–7759 (2021).
- 22. Kim, B. et al. Intravoxel incoherent motion diffusion-weighted imaging of the pancreas: Characterization of benign and malignant pancreatic pathologies. J. Magn. Reson. Imaging 45(1), 260–269 (2017).
- 23. Barral, M. *et al.* Diffusion-weighted MR imaging of the pancreas: Current status and recommendations. *Radiology* **274**(1), 45–63 (2015)
- 24. Sorace, A. G. *et al.* Repeatability, reproducibility, and accuracy of quantitative mri of the breast in the community radiology setting.
- J. Magn. Reson. Imaging https://doi.org/10.1002/jmri.26011 (2018).

 25. Jiang, J. et al. Lung cancer: Short-term reproducibility of intravoxel incoherent motion parameters and apparent diffusion coefficient
- at 3T. J. Magn. Reson. Imaging 47(4), 1003–1012 (2018).
- 26. Weller, A. et al. Diffusion-weighted (DW) MRI in lung cancers: ADC test-retest repeatability. Eur Radiol. 27(11), 4552-4562 (2017).
- 27. Kakite, S. *et al.* Hepatocellular carcinoma: Short-term reproducibility of apparent diffusion coefficient and intravoxel incoherent motion parameters at 3.0T. *J. Magn. Reson. Imaging* **41**(1), 149–156 (2015).
- 28. Rosenkrantz, A. B., Oei, M., Babb, J. S., Niver, B. E. & Taouli, B. Diffusion-weighted imaging of the abdomen at 3.0 Tesla: Image quality and apparent diffusion coefficient reproducibility compared with 15 Tesla. J. Magn. Reson. Imaging 33(1), 128–135 (2011).
- 29. Chen, S. et al. Repeatability of apparent diffusion coefficient at 3.0 Tesla in normal pancreas. Cureus 13(6), 15734–15816 (2021).
- 30. Ye, X. H., Gao, J. Y., Yang, Z. H. & Liu, Y. Apparent diffusion coefficient reproducibility of the pancreas measured at different MR scanners using diffusion-weighted imaging. *J. Magn. Reson. Imaging* 40(6), 1375–1381 (2014).
- 31. Braithwaite, A. C., Dale, B. M., Boll, D. T. & Merkle, E. M. Short- and midterm reproducibility of apparent diffusion coefficient measurements at 3.0-T diffusion-weighted imaging of the abdomen. *Radiology* **250**(2), 459–465 (2009).
- 32. Taouli, B. et al. Diffusion-weighted imaging outside the brain: Consensus statement from an ISMRM-sponsored workshop. J. Magn. Reson. Imaging 44(3), 521–540 (2016).
- 33. Dale, B. M., Braithwaite, A. C., Boll, D. T. & Merkle, E. M. Field strength and diffusion encoding technique affect the apparent diffusion coefficient measurements in diffusion-weighted imaging of the abdomen. *Invest Radiol.* 45(2), 104–108 (2010).
- 34. Zhang, Y. et al. Preliminary experience of 5.0 T higher field abdominal diffusion-weighted MRI: Agreement of apparent diffusion coefficient with 3.0 T imaging. J. Magn. Reson. Imaging 56(4), 1009–1017 (2022).
- 35. Zheng, L. et al. T2-weighted MRI and reduced-FOV diffusion-weighted imaging of the human pancreas at 5 T: A comparison study with 3 T. Med. Phys. 50(1), 344–353 (2023).
- 36. Schoennagel, B. P. et al. Diffusion-weighted imaging of the healthy pancreas: Apparent diffusion coefficient values of the normal head, body, and tail calculated from different sets of b-values. J. Magn. Reson. Imaging 34(4), 861–865 (2011).
- 37. Yoshikawa, T. et al. ADC measurement of abdominal organs and lesions using parallel imaging technique. AJR Am. J. Roentgenol. 187(6), 1521–1530 (2006).
- 38. Wang, J., Ma, C., Yang, P., Wang, Z., Chen, Y., Bian, Y., Shao, C., Lu, J. Diffusion-weighted imaging of the abdomen: Correction for gradient nonlinearity bias in apparent diffusion coefficient. *J. Magn. Reson. Imaging*, (2022).
- 39. Malyarenko, D. I. *et al.* Demonstration of nonlinearity bias in the measurement of the apparent diffusion coefficient in multicenter trials. *Magn. Reson. Med.* 75(3), 1312–1323 (2016).
- 40. In't Veld, P. & Marichal, M. Microscopic anatomy of the human islet of Langerhans. Adv. Exp. Med. Biol. 654, 1-19 (2010).
- 41. Allisy-Roberts, P. J., Williams J. Farr's physics for medical imaging[M]. (Elsevier Health Sciences, 2007).

Author contributions

Z.J.: Conceptualization, Methodology, Formal analysis, Data curation, Writing-original draft. W.S.: Data curation, Resources, Validation, Writing-review & editing. D.X.: Data curation, Investigation. H.Y.: Conceptualization, Methodology, Data curation, Validation. H.M.: Visualization, Software. X.S.: Supervision, Writing-review & editing. H.X.: Conceptualization, Methodology, Formal analysis, Investigation, Writing-review & editing, Project administration. Z.J. and W.S. have the equal contribution.

Competing interests

The authors declare no competing interests.

Additional information

Correspondence and requests for materials should be addressed to X.S. or H.X.

Reprints and permissions information is available at www.nature.com/reprints.

Publisher's note Springer Nature remains neutral with regard to jurisdictional claims in published maps and institutional affiliations.

Open Access This article is licensed under a Creative Commons Attribution 4.0 International License, which permits use, sharing, adaptation, distribution and reproduction in any medium or format, as long as you give appropriate credit to the original author(s) and the source, provide a link to the Creative Commons licence, and indicate if changes were made. The images or other third party material in this article are included in the article's Creative Commons licence, unless indicated otherwise in a credit line to the material. If material is not included in the article's Creative Commons licence and your intended use is not permitted by statutory regulation or exceeds the permitted use, you will need to obtain permission directly from the copyright holder. To view a copy of this licence, visit http://creativecommons.org/licenses/by/4.0/.

© The Author(s) 2023